

NUMERICAL STUDY FOR OSCILLATORY FLOW PAST THREE-CYLINDER ARRAY IN REGULAR TRIANGLE ARRANGEMENT USING DIRECT-FORCING IMMERSED BOUNDARY METHOD

M.J. Chern^{*1} Y.L. Chen^{*} C.B. Liao^{**} T.L. Horng^{***}

^{*} Department of Mechanical Engineering, National Taiwan University of Science and Technology

^{**} Department of Water Resources Engineering and Conservation, Feng Chia University

^{***} Department of Applied Mathematics, Feng Chia University

Keywords: Direct-Forcing Immersed Boundary Method, Circular Cylinder Array, Oscillatory Flow, Fluid-Structure Interaction

ABSTRACT

The interaction between structures and fluid flow receives more attention in offshore engineering in the past decades. For example, the simulation of an oscillatory flow past a cylinder array is used to predict the hydrodynamic loading of a tension-leg platform (TLP) from progressive waves. A TLP usually has more than one cylinder as the framework to encounter oscillatory flow from waves. However, the design of an array of three cylinders in a regular triangle arrangement in oscillatory flow is rarely studied. Therefore, the main objective of this study is to present the simulation of the interaction between the oscillatory flow and arrays of three cylinders in a triangular arrangement using the direct forcing immersed boundary method. A virtual force based on the rate of momentum changes of a solid body is added to the momentum equations of fluid. Consequently, this method can solve the force caused by the solid body immersed in fluid cells.

In this study, the results include the effects of Keulegan-Carpenter number (KC), pitch ratio (P/D), and symmetry of the arrangement. The difference between arrays of three and four cylinders is investigated. The arrangement of the array of four cylinders is similar to the array of three cylinders that all cylinders are symmetric with respect to the in-line direction. The proposed approach can be useful for scientists and engineers who would like to understand the interaction of the oscillatory flow with the cylinder array or to estimate hydrodynamic loading on the array of cylinders.

INTRODUCTION

Oscillatory flow past structures often occurs in nature and numerous engineering application. For example, the offshore pipeline has been widely used to transport the oil and gas products on the seabed. Since these structures are in the offshore region, it is important to predict hydrodynamic loadings from waves and currents. Another example is a tension-leg platform (TLP) which is commonly used for petroleum en-

gineering and wind energy engineering. A TLP usually has more than one cylinder as the framework to encounter oscillatory flow from waves. However, these cylinders are huge and heavy so the costs of construction are relatively expensive. If fewer cylinders are utilized as a framework of the TLP, then the cost will be reduced and improve construction efficiency. This idea would be achieved as we focus on the design of array of three cylinders in a regular triangle arrangement. It should be noticed that the arrangement of cyl-

¹ Corresponding author (mjchern@mail.ntust.edu.tw)

ylinder array is an important impact factor of hydrodynamic loadings. In recent years, the configuration of three cylinders in a regular triangle arrangement is commonly used for the offshore power station. The numerical study of this arrangement of cylinder array in uniform flow was presented by Bao *et al.* [1]. The effect of gap spacing and incidence angle on the flow patterns around cylinders are shown in their paper. Nevertheless, research on oscillatory flow past three cylinders in an equilateral arrangement is rare.

Past experimental studies concerned with an oscillatory flow interaction with a single circular cylinder were conducted by several researchers. Sarpkaya [2] provided theoretical and experimental results of inertia in-line force coefficient and flow visualization. Obasaju *et al.* [3] measured the force and span wise correlation of vortex shedding for a circular cylinder in the planar oscillatory flow. It is known that Keulegan-Carpente (KC) number has a great influence on the vortex shedding regimes. A dimensionless parameter referred to KC number $U_m T / D$ is used to express the stroke ($U_m T$) of the orbital motion of fluid particles in relation to the diameter (D) of the cylinder. The development of flow at KC number from 4 to 55 is classified into five categories which are as symmetric, the transverse, the diagonal, the third vortex and the quasi-steady regimes. Sumer and Fredsoe [4] reviewed several previous studies and described the flow pattern and the resulting loading when waves interact with a cylinder.

Since computing technology has been improved dramatically in recent decades, more researchers used numerical methods to study the interaction between the oscillatory flow and cylinders. Illiadis and Anagnostopoulos [5] investigated the oscillatory flow around a circular cylinder at low KC by solving vorticity-stream function approach of Navier-Stokes equation. They used vorticity contours to show the results of flow visualization and predicted the in-line and transverse forces on the cylinder. An *et al.* [6] investigated the oscillatory flow past two cylinders in a tandem arrangement. They found that the effect of KC and gap ratio on cylinders by observing flow characteristics and force variations. Chern *et al.* [7] simulated the interaction of oscillatory flow with a pair of side-by-side square cylinders. They used phase diagrams of

force components and spectral analysis to describe the chaotic flow. Anagnostopoulos and Dikarou [8] and Chern *et al.* [9] provided the numerical studies of arrays of four cylinders in oscillatory flow. They reported the effect of pitch ration and KC number by showing hydrodynamic force on the cylinders and vorticity contours. Zhong and Wang [10] used a time-accurate stabilized finite-element method to approximate the three dimensional interaction between the solitary waves and a single cylinder or an array of four cylinders.

The immersed boundary method (IB method) has been getting popular in the recent years since it was introduced by Peskin [11]. The IB method has a great capability to handle complex geometry and moving body due to its utilization of meshes is a fixed Cartesian grid for a fluid and Lagrangian grid for an immersed boundary. This method uses a Dirac delta function to get the relative force between fluid and immersed body. A novel IB method called direct-forcing method was proposed by Mohd. Yusof [12]. The direct-forcing method determines a forcing term by calculating the difference between the interpolated velocities on the boundary points and the desired solid boundary velocities. Numerous researchers adopted the ideal of direct-forcing method and reported many successful applications. Noor *et al.* [13] used the direct-forcing immersed boundary method to simulate a number of benchmark problems for both stationary and moving solid object in uniform flow. Chern *et al.* [14] also used this direct-forcing immersed boundary method to present the oscillatory flow past an array of four cylinders successfully. Kampe and Frohlich [15] proposed an improved direct-forcing immersed boundary method to enhance the results. They developed an additional forcing scheme to improved coupling of solid and fluid phase. Chern *et al.* [16] extended the idea of virtual force to virtual heat. They successfully applied the virtual heat concept to mixed heat transfer problems.

The main objective of this study is to present the simulation of the interaction between the oscillatory flow and the arrays of three cylinders in a regular triangle arrangement by using the direct forcing immersed boundary method. In order to proof that the design of an array of three cylinders in a regular triangle

arrangement can provide a stable condition like the array of four cylinders in the offshore region, this results are compared with the array of four cylinders in a square arrangement in the oscillatory flow.

MATHEMATICAL FORMULAE AND NUMERICAL MODEL

1. Problem Descriptions

It is known that the flow around multiple cylinders is more complex than that around a single cylinder. To demonstrate that our in-house numerical code gives stable and accurate results, an oscillatory flow past a single cylinder is considered as the benchmark test problem. This benchmark test study has already been validated successfully by Chern *et al.* [9]. Therefore, the method from their study for validation and the grid independence is adopted. In the present study, a single cylinder is located at the center of the computational domain. The computational domain size is $25D \times 20D$. The schematic and boundary conditions are depicted in Fig. 1(a). These numerical results are compared with other standard cases by Illiadis and Anagnostopoulos [5]. Simulations are done for $KC = 2$ and 10 both $Re = 200$.

2. Governing Equations

Water is the fluid in the present study. It is customary to regard water as incompressible viscous fluid, so the dimensionless equations of continuity and momentum can be denoted as

$$\nabla \cdot \mathbf{u} = 0 \quad (1)$$

and

$$\frac{\partial \mathbf{u}}{\partial t} + \nabla \cdot (\mathbf{u}\mathbf{u}) = -\nabla p + \frac{1}{Re} \nabla^2 \mathbf{u} + \mathbf{f} \quad (2)$$

where \mathbf{u} and p are dimensionless velocity and pressure, respectively. Re is Reynolds number given by $U_m D / \nu$, where U_m is the magnitude of the imposed oscillatory flow velocity, D is the cylinder diameter and ν is the kinematic viscosity of the water. In order to accommodate interaction between solid and fluid, a virtual force term \mathbf{f} is added in Eq. (2). It is determined by

$$\mathbf{f} = \eta \frac{\mathbf{u}_s - \mathbf{u}}{\Delta t}, \quad (3)$$

where η is a function to distinguish the solid and fluid in the computational cell and η equal to 1 or 0 for solid or fluid cells, respectively. For example, there is

a circular cylinder in the flow domain. Given that the distance between the center of cylinder and the center of cell is less than the radius of the cylinder, then η will be 1. On the other hand, η is 0 when the distance is greater the radius. \mathbf{u}_s is the velocity of solid.

3. Oscillatory Flow Boundary Condition

We consider oscillatory flow in order to simulate the flow of shallow wave motion (see [17]). The time-dependent dimensionless velocity boundary conditions are imposed at four boundaries as

$$u = \sin \frac{2\pi t}{T} \text{ and } v = 0, \quad (4)$$

where T is the period of oscillatory flow.

4. Numerical Procedures

The three-step time-split scheme is used to solve

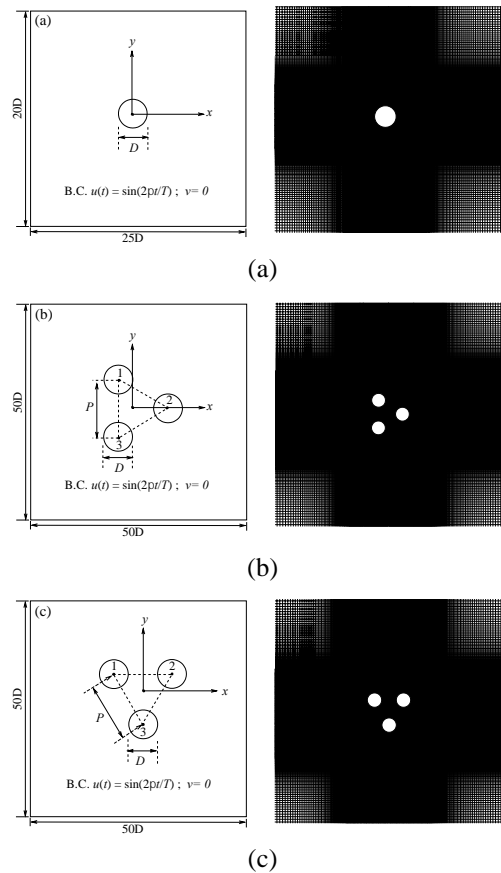


Fig. 1 Schematics of interaction of an oscillatory flow past (a) a single cylinder, (b) the array of three cylinders in the symmetric configuration, and (c) the array of three cylinders in the asymmetric configuration and enlargement of non-uniform grids.

the momentum equation Eq. (2). In the beginning, the velocity is stepped from the m^{th} time level to the intermediate level “*” by solving the advection-diffusion equations without the pressure gradient and the virtual force term. This following step is discretized by third-order Adam-Bashforth method,

$$\frac{\mathbf{u}^* - \mathbf{u}^m}{\Delta t} = \frac{1}{12} (23S^m - 16S^{m-1} + 5S^{m-2}), \quad (5)$$

where S includes the convective and diffusive terms of the momentum equations in Eq. (2). The intermediate velocity in Eq. (5) does not satisfy the continuity equation, Eq. (1), since the pressure gradient term and the virtual force are not included in Eq. (5). At the second step, \mathbf{u}^* is marched to the second intermediate velocity \mathbf{u}^{**} by including the pressure gradient term

$$\frac{\mathbf{u}^{**} - \mathbf{u}^*}{\Delta t} = -\nabla p^{m+1}. \quad (6)$$

and applying the divergence of Eq. (6) gives

$$\frac{\nabla \cdot \mathbf{u}^{**} - \nabla \cdot \mathbf{u}^*}{\Delta t} = -\nabla^2 p^{m+1}. \quad (7)$$

The second intermediate velocity \mathbf{u}^{**} should satisfy the continuity equation, i.e.

$$\nabla \cdot \mathbf{u}^{**} = 0. \quad (8)$$

Then substitution of Eq. (8) to (7) gives the Poisson equation

$$\nabla^2 p^{m+1} = \frac{1}{\Delta t} \nabla \cdot \mathbf{u}^*. \quad (9)$$

After solving the Poisson equation of pressure, the second intermediate velocity \mathbf{u}^{**} can be advanced in Eq. (6). In the final step, the virtual force term is imposed in the following equation Eq. (10) so the velocity \mathbf{u}^{m+1} can be updated,

$$\frac{\mathbf{u}^{m+1} - \mathbf{u}^{**}}{\Delta t} = \mathbf{f}^{m+1}. \quad (10)$$

The term \mathbf{f} in Eq. (10) represent the action of a solid upon a fluid. For the solid, it can be regarded as the force to hold or to drive a solid when it is stationary or moving. In contrast, there is no virtual force between the fluid cells because η is 0. In order to satisfy the no-slip boundary condition at the fluid-solid interface, the force acting on the solid should insure that the fluid velocity \mathbf{u} is equal to the solid velocity \mathbf{u}_s at the $(m+1)^{\text{th}}$ time step, i.e. $\mathbf{u}^{m+1} = \mathbf{u}_s^{m+1}$. Therefore, the

virtual force is defined as the rate of momentum changes of solid body and proportional the difference between the solid velocity at the $(m+1)^{\text{th}}$ time step and the fluid velocity at the m^{th} time step.

In this study, the finite volume method is used to solve the momentum equation. A staggered grid is used to accommodate velocity and pressure separately in a computational cell. The advective scheme is discretized by the third order QUICK scheme. Non-uniform grids 250×220 and 420×420 grids are used for a single cylinder and three cylinders, respectively. The tightly area adopts $\Delta x = \Delta y = 0.028$. The time increment $\Delta t = 10^{-3}$ satisfies with the CFL condition. The convergence criterion of 10^{-4} for the maximum mass residual is considered in this study. The total dimensionless time of the simulation is 230. It takes about 2 days for a simulation of 2-D oscillatory flow around a single cylinder at a PC cluster consisting of Intel Xeon E31220 V2 3.10 GHz.

5. Calculation of Hydrodynamic Force on Cylinder

We use the volume integral over the cylinder volume to calculate the forces acting on the immersed body that can be shown as

$$\mathbf{F} = \iiint_{\Omega_s} \mathbf{f} dV. \quad (11)$$

The in-line and transverse force coefficients, C_f and C_t can be determined by

$$C_f = -2F_x \quad (12)$$

and

$$C_t = -2F_y, \quad (13)$$

respectively. The root-mean-square value of in-line and transverse force coefficients are defined as

$$\bar{C}_f = \left(\frac{1}{T} \int_0^T C_f^2 dt \right)^{1/2} \quad (14)$$

and

$$\bar{C}_t = \left(\frac{1}{T} \int_0^T C_t^2 dt \right)^{1/2} \quad (15)$$

6. Grid Independence and Validation

Fig. 2(a) shows that we use a number of grid systems to obtain grid independent solutions for oscillatory flow past a single cylinder at $KC = 2$ and $Re = 200$.

The evolution of predicted wake length is in good agreement with Illiadis and Anagnostopoulos [5]. As we can see, the results by grids 250×220 and grids 290×250 are very similar and more accurate than grids 150×130 . In order to ensure the accuracy and save time for computation, 250×220 grids are adopted in present study.

Furthermore, the time histories of C_f are compared with Illiadis and Anagnostopoulos [5] in Fig. 2 (b) and (c), where $KC = 2$ and 10 respectively. The results show that the value C_f will reach maximum when flow change its direction and the C_f decreases as the KC number increases. The present results are in good agreement with measured value. It turns out that our numerical model is capable to simulate the interaction of oscillatory flow with a single cylinder and prediction of hydrodynamic loading is reliable.

RESULTS AND DISCUSSION

In this study, two kinds of configurations of three cylinders in a regular triangle arrangement are considered. The schematics are shown in Fig. 1(b) and (c), respectively. The array of cylinders is located at the center of the computational domain. The size of computational domain is $50D \times 50D$. This large domain can prevent the reflection of vortices from boundaries since vortices are dissipated by fluid viscosity before they reach boundaries. The gap between two centers of cylinders is denoted by P . The enlargements of the grids are shown in the right hand side of Fig. 1. The first arrangement of the array is the so-called symmetric configuration which is symmetric with respect to the in-line direction. In contrast, the second arrangement is the asymmetric configuration. Several effects on the interaction of the oscillatory flow with the arrays of 3 cylinders and the difference between the arrays of three and four cylinders are discussed in the following sections.

1. Effect of KC Number

In this section, the effect of Keulegan-Carpenter (KC) number, $U_m T / D$, in the symmetric configuration on the oscillatory flow is discussed. The vorticity contours, hydrodynamic coefficients and spectrum analysis are used to explain the interaction between oscillatory flow and the array of 3 cylinders in the symmetric configuration at various KC numbers. In this study,

KC varies from 3 to 10, $P/D = 2$ and Re is fixed at 200.

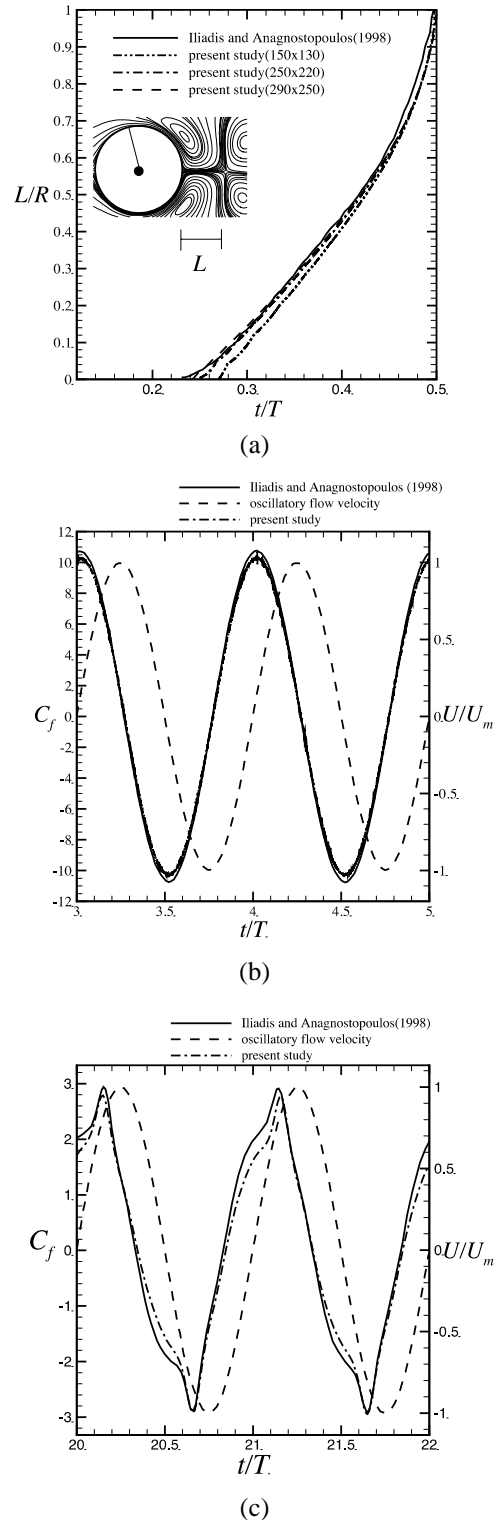


Fig. 2 Grid independence at (a) $KC = 2$. Time histories of C_f at (b) $KC = 2$ and (c) $KC = 10$, where $Re = 200$.

1.1 Flow Patterns

The vorticity contours during a cycle at $KC = 3$ and $P/D = 2$ are shown in Fig. 3(a). As the KC value is low, the pairs of vortices occur alternatively in two sides of cylinders and are attached on each cylinder. The flow pattern is symmetric with respect to the in-line direction. As KC increases to 5, the flow pattern is still symmetric with respect to the in-line direction as shown in Fig. 3(b). However, the vortices around

the lateral cylinders 1 and 3 become asymmetric with respect to their in-line direction. The inner vortices adjacent to the central gap of the array are longer than the outer vortices. The symmetries of vortices around these cylinders are broken due to that there is enough time for vortices start to shed at $KC = 5$. When $KC = 8$ as shown in Fig. 4, the vortical systems become more chaotic and asymmetric than the case of $KC = 5$. More asymmetric vortices are generated in the beginning of

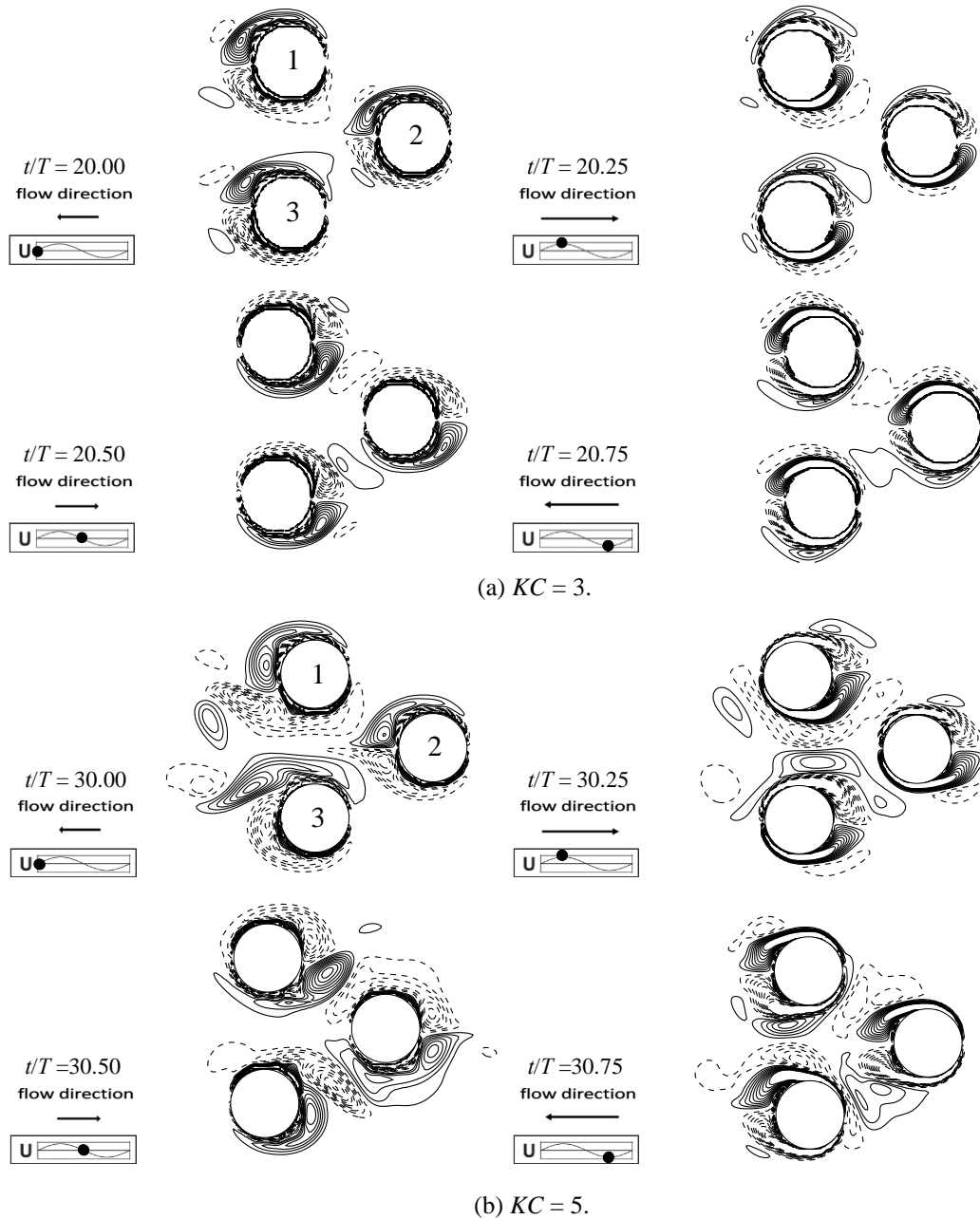


Fig. 3 Vorticity contours of the oscillatory flow interacting with the array of three cylinders in the symmetric configuration during a cycle at $Re = 200$ and $P/D = 2$.

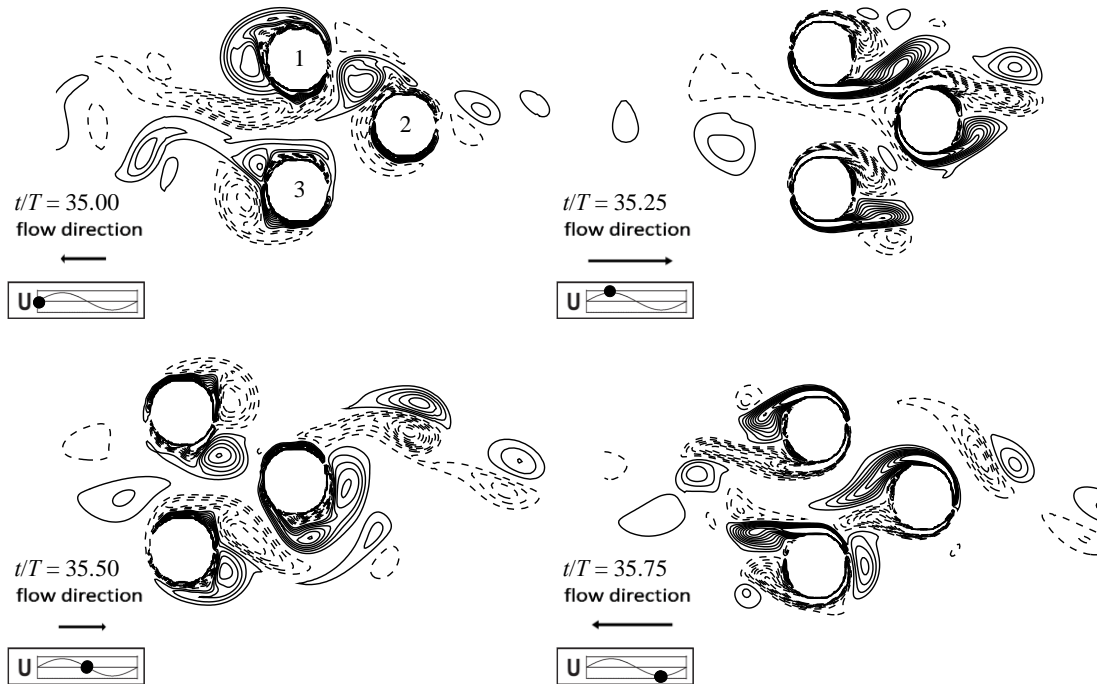


Fig. 4 Vorticity contours of the oscillatory flow interacting with the array of three cylinders in the symmetric configuration during a cycle, where $KC = 8$, $Re = 200$, $P/D = 2$.

cycle. Subsequently, the pair of vortices shed away from cylinders as time marches. In the next of half cycle, number of shedding vortices are drawn back to attach cylinders again. For the high KC number, the interaction among three cylinders is strong because the vortices are not damped until they travel farther from cylinders.

1.2 Variation of C_f with KC

Fig. 5 shows the time histories of the in-line force coefficient C_f of the cylinders 1 and 2 at various KC numbers. At the same KC , the variations of C_f are similarly sinusoidal for all cylinders. The maximum occurs at $KC = 3$ in Fig. 5(a) and C_f decreases as KC increases. It is hard to discover the difference of C_f between different cylinders when KC number is low. As KC number raises to 8, the sinusoidal form of C_f is not regular any more as shown in Fig. 5(c). For a high KC number, the amplitudes of C_f on cylinders 1 and 2 are slightly different when the oscillatory flow changes its direction.

1.3 Variation of C_l with KC

Fig. 6 displays the time histories and spectrum analyses of C_l on cylinders 1 and 2 at various KC num-

bers. When KC is 3 in Fig. 6(a), the variations of C_l on cylinders 1 and 2 are sinusoidal. The amplitude of C_l on the cylinder 1 is higher than the cylinder 2 because the position of cylinder 2 is on the horizontal central line of the symmetric configuration. Since vortex motion around the cylinder 2 is almost symmetric with respect to the horizontal central line as shown in Fig. 3(a), C_l does not vary significantly. According to the spectral analyses of C_l , the ratios of fundamental frequency of C_l to the frequency of the oscillatory flow are 1 for all cylinders. It means the fundamental frequency of C_l and that of the oscillatory flow are equal. C_l has the same fundamental frequency with the oscillatory flow because the variation of C_l is dominated by the oscillatory flow and only symmetric vortex pairs alternatively occurring in two sides of the cylinders cause the variation of C_l . The symmetric vortex pairs do not shed away from cylinders and only change their directions of vortex pairs with the oscillatory flow. As KC increases to 5 in Fig. 6(b), C_l of cylinder 1 becomes irregular and higher than the case at $KC = 3$, but the C_l of cylinder 2 is still as low as the case at $KC = 3$. The ratios of fundamental frequency of C_l on cylinders 1 and 2 shift from 1 to 2 as KC increases to 5.

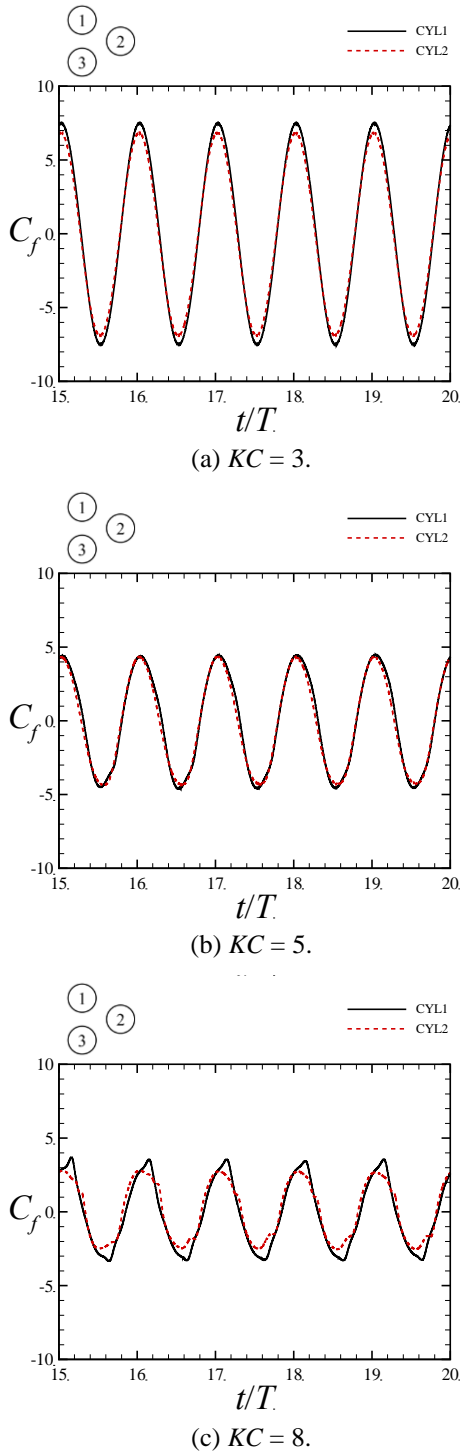


Fig. 5 Time histories of C_f on the cylinders 1 and 2 in the symmetric configuration at $P/D = 2$ and $Re = 200$.

This jump in the ratio of fundamental frequency is due to the occurrence of vortex shedding when KC increases to 5. As KC is raised to 8 in Fig 6(c), the

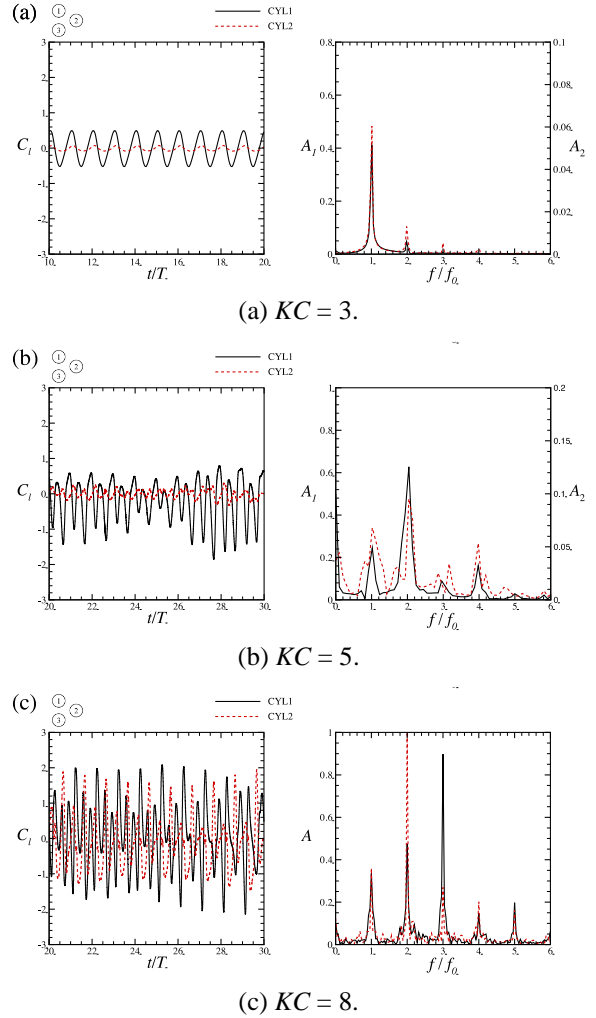
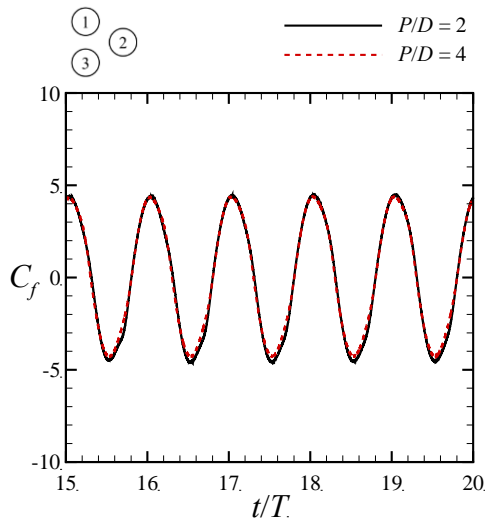
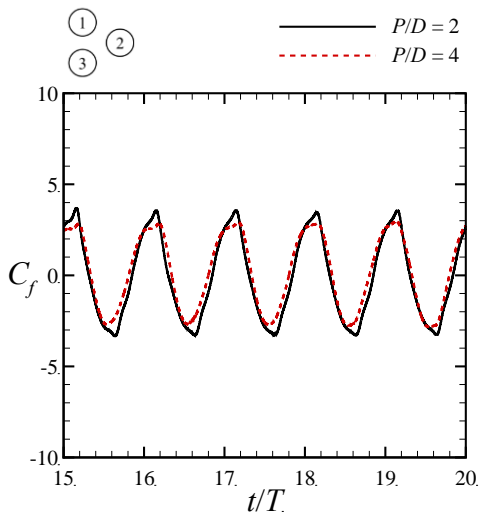


Fig. 6 Time histories and spectrum analyses of C_l on the cylinders 1 and 2 in the symmetric configuration at $P/D = 2$ and $Re = 200$.

amplitudes of C_l on cylinders 1 and 2 become larger than the case of $KC = 5$. The variations of C_l on both cylinders 1 and 2 are more irregular and higher than the cases at $KC = 5$. The ratios of fundamental frequency of C_l on cylinders 1 are increased to 3 when $KC = 8$. All of these results imply that the form of vortex shedding has a direct effect on the variation of C_l . The vortices are symmetric and appear alternatively in two sides of a cylinder when KC is low so the ratio of fundamental frequency of C_l is 1. When KC number increases, the vortices become asymmetric, start to shed, and more vortices travel away from cylinders in a half of oscillatory cycle. These asymmetric vortices let the frequency of C_l becomes faster than the frequency of the oscillatory flow.



(a) $KC = 5$.



(b) $KC = 8$.

Fig. 7 Time histories of C_f on the cylinder 1 in the symmetric configuration at $P/D = 2$ and 4 and $Re = 200$.

2. Effect of Pitch Ratio

The pitch ratio P/D is one of important factors when a cylinder array is designed in an offshore platform. An offshore platform usually has a basic P/D that can provide enough space for the facilities on the platform. The gap among cylinders cannot be too small. Therefore, two pitch ratios as 2 and 4 are considered to investigate the effects of pitch ratio on an oscillatory flow past an array of 3 cylinders in the symmetric configuration at $KC = 5$ and 8 and $Re = 200$. Fig. 7 shows the time histories of C_f exerted on the cylinder 1 with a variety of pitch ratios at $KC = 5$ and

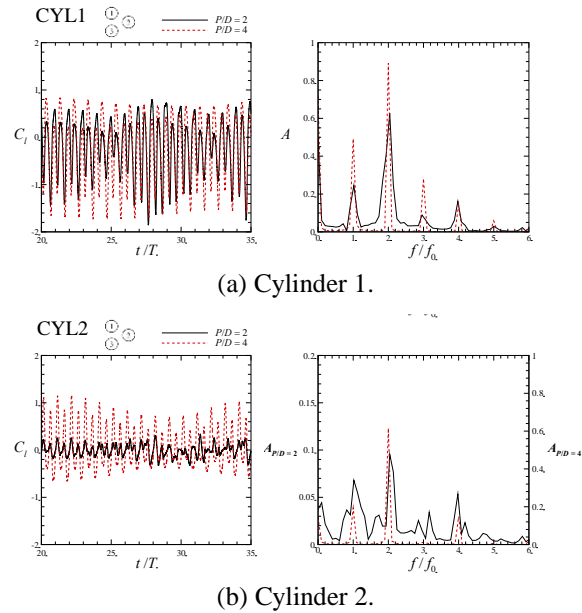


Fig. 8 Time histories and spectrum analyses of C_l on the cylinders in the symmetric configuration at $P/D = 2$ and 4 , $KC = 5$, and $Re = 200$.

8. It seems that C_f is not affected obviously by P/D . As we mentioned before, C_f decreases as the KC number increases. Fig. 8 shows the time histories and spectral analyses of C_l on cylinders 1 and 2 with a variety of pitch ratios at $KC = 5$. For the cylinder 1, the amplitude of C_l ascends as P/D increases from 2 to 4. The fluctuation of C_l on the cylinder 1 at $P/D = 2$ is more obvious than the case of $P/D = 4$ because the interaction among there cylinder is strong when the P/D value is low. The ratios of the fundamental frequency of C_l to the oscillator flow frequency at both pitch ratios are 2. For the cylinder 2, the amplitude of C_l also increases as P/D increases. The ratios of the fundamental frequency of C_l at $P/D = 2$ and 4 are 2. It should be noted that the interaction between different P/D does not affect the ratios of the fundamental frequency of C_l at $KC = 5$. The results are contrary at $KC = 8$ in Fig. 9. For both cylinders 1 and 2, the amplitudes of C_l become smaller as P/D increases from 2 to 4. The ratio of the fundamental frequency of C_l on the cylinder 1 is changed from 3 to 2 as P/D increases. In the other hand, the ratios of the fundamental frequency of C_l on the cylinder 2 at both P/D as 2 and 4 are 2. These results imply that the interaction among three cylinders at $KC = 8$ is stronger than the case of $KC = 5$. The ratio of the fundamental frequency of C_l on cylinder 1

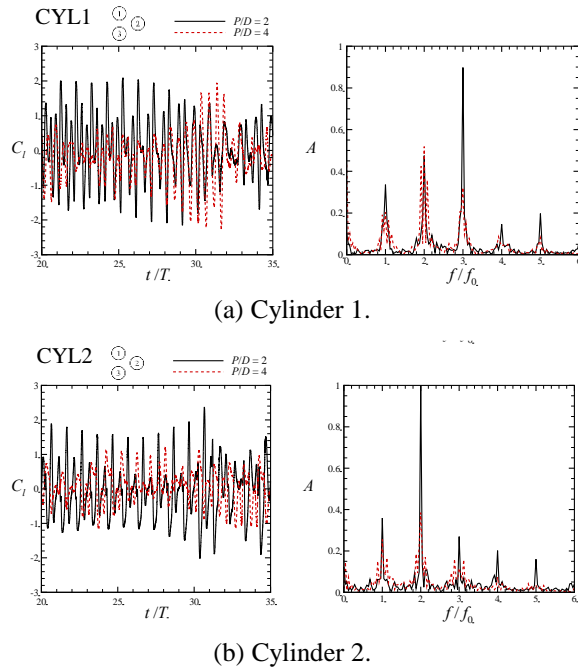


Fig. 9 Time histories and spectrum analyses of C_l on the cylinders in the symmetric configuration at $P/D = 2$ and 4 , $KC = 8$, and $Re = 200$.

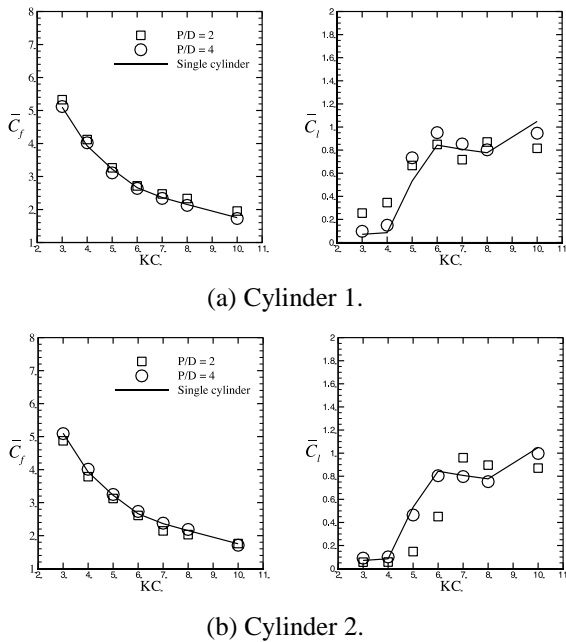


Fig. 10 R.M.S. value of C_f and C_l in the symmetric configuration versus KC on cylinders and only a single cylinder at different P/D .

is higher when P/D is as low as 2. When $KC = 8$, increasing P/D from 2 to 4 let the interaction among three cylinders becomes weak so ratios of the funda-

mental frequency of C_l on different cylinders are consistent as 2. The results show that C_f is almost the same even P/D increases, but C_l and its fundamental frequency change with respect to P/D . The root mean square value of in-line force and transverse force coefficients \bar{C}_f and \bar{C}_l of cylinder 1 and 2 at different P/D and KC values are presented in Fig. 10. In order to investigate the difference between the present array of 3 cylinders and the case of a single cylinder in the oscillatory flow, \bar{C}_f and \bar{C}_l of the single cylinder are shown in Fig. 10. For the both P/D values, 2 and 4, \bar{C}_f of the cylinders 1 and 2 have an identical variation that decreases as KC increases. These results of the cylinders 1 and 2 are consistent with the case of a single cylinder in the oscillatory flow. Consequently, the extremely influential factor of C_f is the KC number. The \bar{C}_l values of the cylinders 1 and 2 at $P/D = 2$ and 4 increase as KC increases. Comparing the results with $P/D = 2$ and 4 for the cylinder 1, the \bar{C}_l of $P/D = 4$ is more similar to the single cylinder except for $KC = 5$ and 6. For various KC numbers, the cylinder 2 has a persistent result that increasing P/D from 2 to 4 can get the consistency of \bar{C}_l with the single cylinder.

3. Effect of Asymmetric Configuration

In order to investigate the effect of asymmetric arrangement of array of three cylinders at $P/D = 2$ in the oscillatory flow, the vorticity contours, hydrodynamic coefficients and spectrum analyses are used to explain. Two KC numbers, 3 and 5, are considered and Re is fixed at 200.

3.1 Flow Patterns

Fig. 11 shows the evolution of vorticity contours around an asymmetric array of three cylinders in a regular triangle arrangement during a cycle. The vortices are almost symmetric with respect to the in-line flow direction at $KC = 3$ in Fig. 11(a). The vortices of the cylinder 3 is slightly asymmetric with respect to the in-line flow direction. All of the vortices occur in the alternating sequence on two sides of those cylinders. This result is the same as the symmetric configuration in the oscillatory flow at $KC = 3$. As KC increases to 5, the vortices start to shed away from cylinders. Vortex shedding is found around cylinders in Fig. 11(b). The interaction of cylinders becomes stronger and the asymmetric variation of vortices is more obvious than

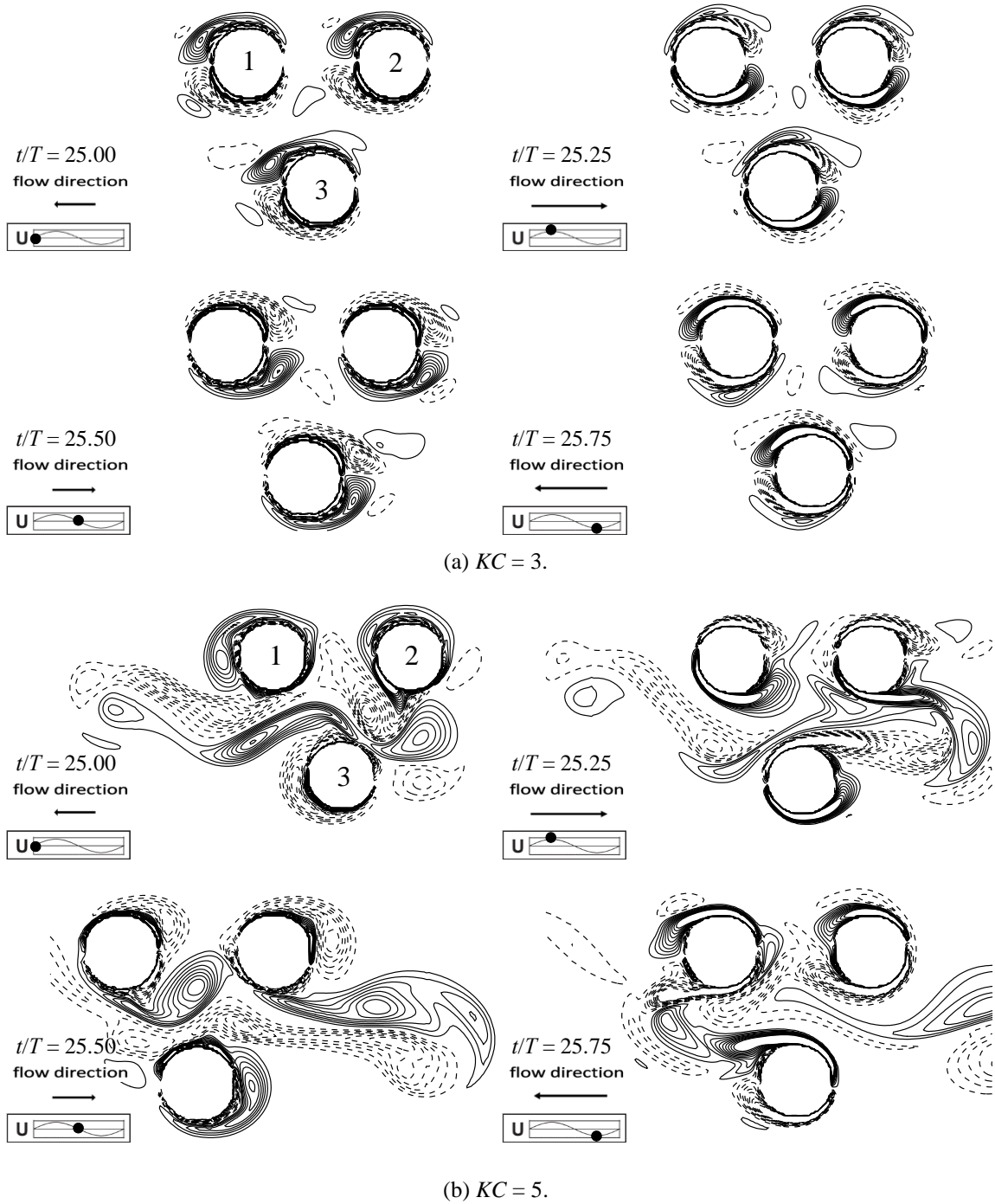


Fig. 11 Vorticity contours of the oscillatory flow interacting with the array of three cylinders in an asymmetric configuration during a cycle at $P/D = 2$ and $Re = 200$.

the case of the symmetric configuration at $KC = 5$.

3.2 Variation of C_f and C_l

Fig. 12 demonstrates the time histories of C_f on the cylinder 1 in the asymmetric configuration. C_f decreases as KC increases from 3 to 5 as shown in Fig.

12(b). C_f of the asymmetric configuration is sinusoidal with the zero mean value. There is almost no difference between the C_f values of the symmetric and asymmetric configuration. The time histories and spectrum analyses of C_l in the different configurations at $KC = 3$ are displayed in Fig.13. In the symmetric

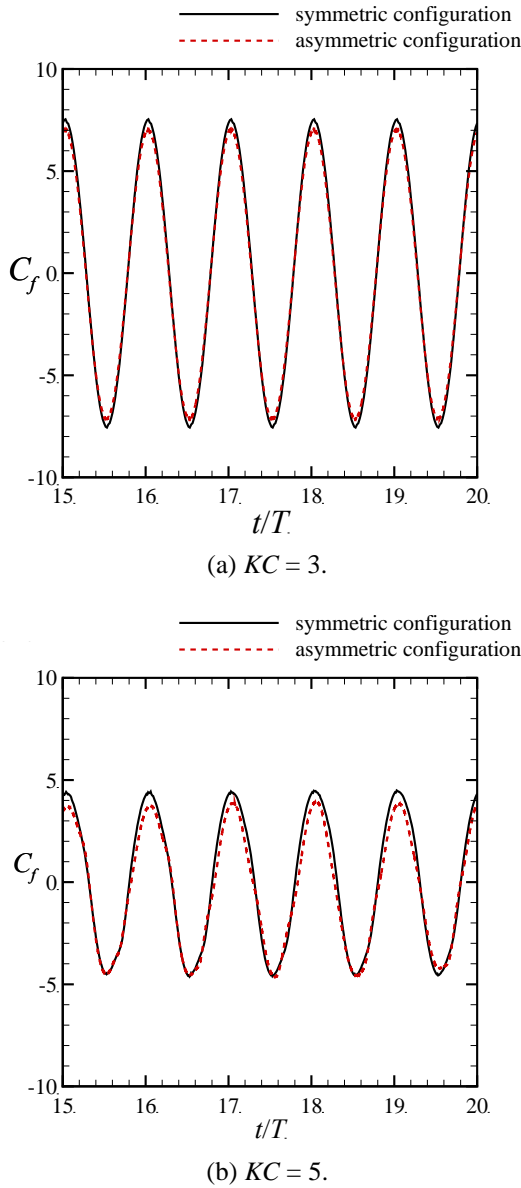


Fig. 12 Time histories of C_f on the cylinder 1 in the different arrays at $P/D = 2$ and $Re = 200$.

configuration, the C_l value of lateral cylinder 1 is higher than the central cylinder 2. In the asymmetric configuration as shown in Fig. 13(b), C_l of the top cylinder 1 is higher than the bottom cylinder 2. The amplitudes of C_l of these configurations are very small because the flow patterns are symmetric with respect to the in-line flow direction. C_l in the symmetric configuration is more symmetric than the asymmetric configuration. According to the spectrum analysis, the ratio of fundamental frequency of C_l in the symmetric configuration is 1. In the asymmetric configuration,

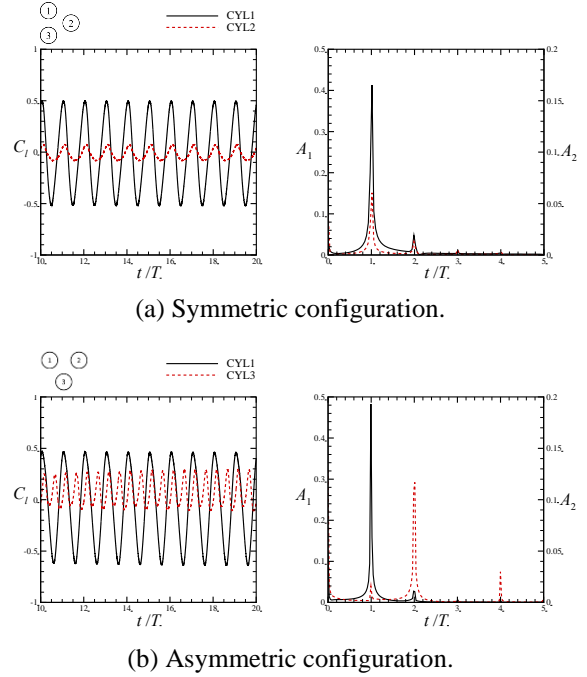


Fig. 13 Time histories of C_l and spectrum analyses on different cylinders at $KC = 3$, $P/D = 2$, and $Re = 200$.

the ratio of fundamental frequency of C_l of the cylinder 3 is 2. We also find that the vortices of cylinder 3 is slightly asymmetric with respect to the in-line direction, so this double ratio of fundamental frequency of C_l of the cylinder 3 is due to the interaction with other cylinders. As KC increases to 5, the discrepancy of C_l between two configurations is obvious as shown in Fig. 14. For the symmetric configuration, the C_l value of the cylinder 2 is almost zero, but there is no such small C_l in the asymmetric configuration. C_l in the asymmetric configuration is higher than in the symmetric configuration since the vortices in the asymmetric configuration shed farther from cylinders. The ratios of fundamental frequency of C_l in two configurations are 2 because the vortices start to shed when $KC = 5$. The harmonic of fundamental frequency in the asymmetric configuration is obviously higher than the symmetric configuration. This result is consistent with the flow pattern and time history of C_l . If the vortex shedding is obvious in the flow pattern, then the amplitude of C_l will also increase higher.

4. Comparison with Array of Four Cylinders in Oblique Flow

In this section, the difference between arrays of

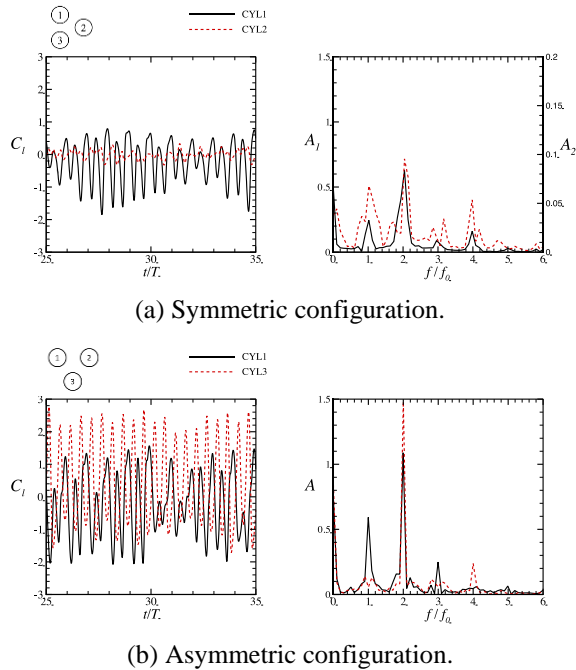


Fig. 14 Time histories of C_l and spectrum analyses on different cylinders at $KC = 5$, $P/D = 2$, and $Re = 200$.

three cylinders and four cylinders in an oscillatory flow is discussed. The arrangement of three cylinders is the symmetric configuration. The array of four cylinders is similar to the array of three cylinders in a symmetric configuration, despite the gap between top and bottom cylinders is slightly longer in the square arrangement. However, the obvious difference of arrangements between these arrays is that there is no cylinder in the left hand side of array of three cylinders. The numerical prediction of the array of four cylinders was presented from [14]. An array of four cylinders was immersed in 45 degree oblique oscillatory flow. For comparing conveniently, the notation of cylinders is recalled in Fig. 17(a). The flow conditions are the same with the array of four cylinders. The first case is set as $KC = 5$, $P/D = 2$ and $Re = 250$. The second case is set as $KC = 10$, $P/D = 2$ and $Re = 500$.

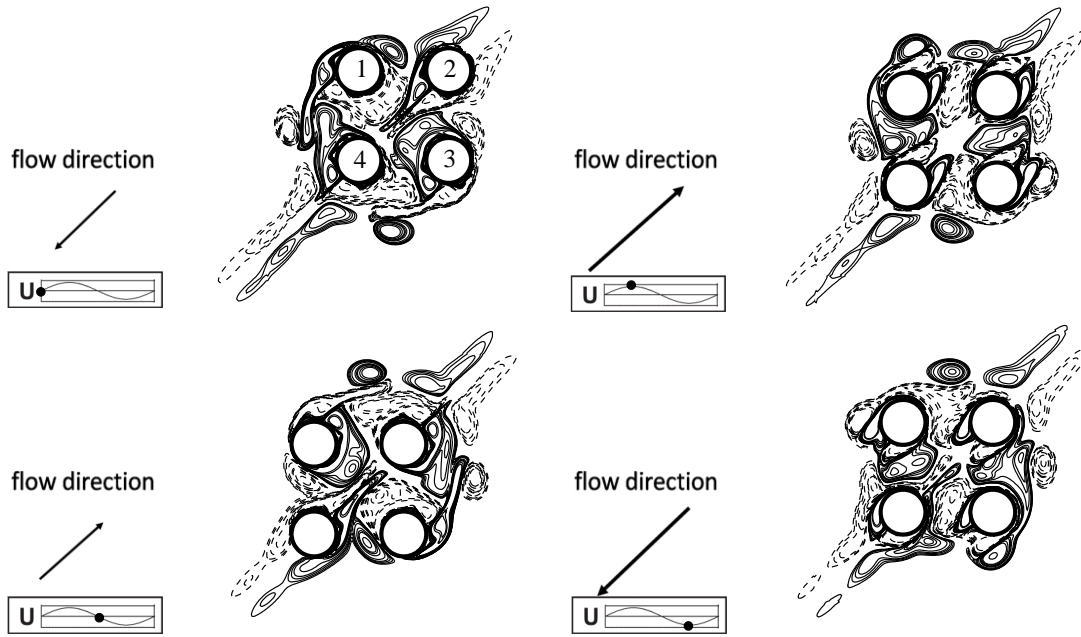
4.1 Flow Patterns

Fig. 15(a) show the evolution of vorticity contours around an array of four cylinders during a cycle. The flow pattern is symmetric with respect to the oblique diagonal line of the domain. This result is different from an oscillatory flow past the array of three cylinders in a regular triangle arrangement, since the

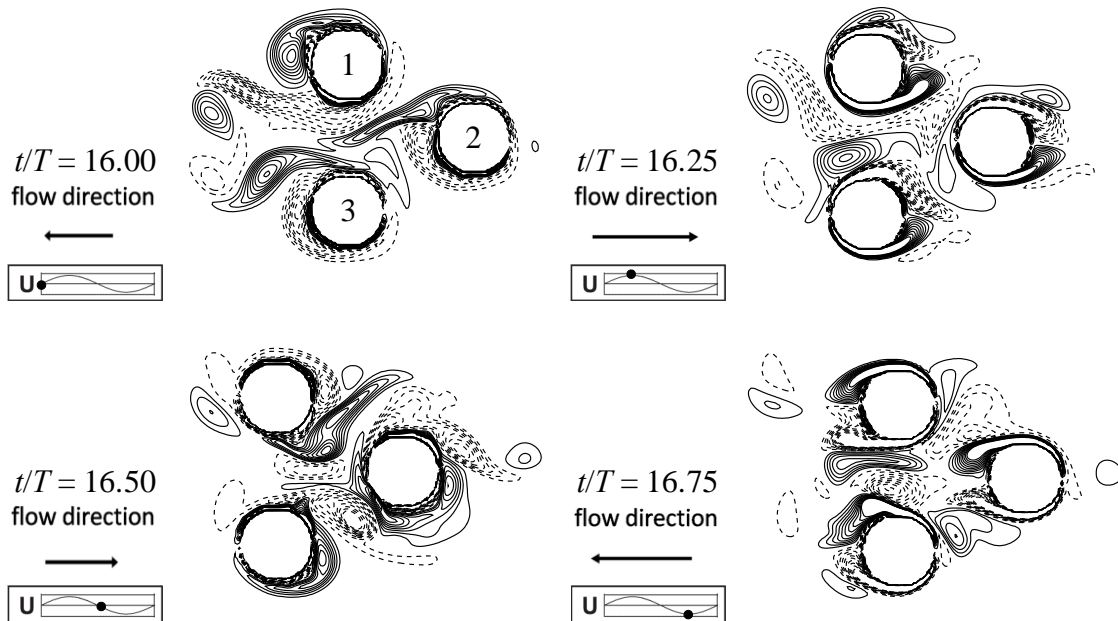
vorticity contours around the array of three cylinders are asymmetric in Fig. 15(b). The asymmetric vortices in an array of three cylinders cause an aperiodicity in the different cycles. In general, the vortical systems of the array of three cylinders in a regular triangle arrangement is quite different with the array of four cylinders at $KC = 5$, $Re = 250$, and $P/D = 2$.

4.2 Variation of C_f and C_l

In order to investigate the effect of different arrangements of arrays between three cylinders and four cylinders in an oscillatory flow, the hydrodynamic loadings in these arrays are compared. C_f on each cylinder of three-cylinder array is almost the same as those results in the array of four cylinders as show in Fig 16. Fig. 17 shows that the time histories of C_l at $KC = 5$ in arrays of three and four cylinders. In the array of four cylinders, C_l of the cylinders 1 and 3 are symmetric with respect to the central horizontal line ($C_l = 0$) and the mean values of C_l on these cylinders are not zero but positive and negative, respectively. The C_l values of the cylinders 2 and 4 in the array of four cylinders do not change significantly. That is, the mean value of C_l values of the cylinders 2 and 4 are almost zero. Therefore, only C_l of cylinder 2 is used to compare with the array of three cylinders. The value of C_l on the cylinders 2 in the array of four cylinders is almost zero. In the array of three cylinders, the C_l values of the cylinders 1 and 3 are asymmetric with respect to the central horizontal line ($C_l = 0$). The C_l value of cylinder 2 in the array of three cylinders is higher than the array of four cylinders. This difference of C_l between arrays of three and four cylinders can be explained by the flow pattern. For the array of four cylinders, the symmetric vortices around the cylinders let the C_l variation become symmetric and regular. However, the asymmetric vortices in the array of three cylinders let the C_l variation become irregular and aperiodic. The spectral analyses of C_l at $KC = 5$ for different arrays are displayed in Fig. 18. The ratios of fundamental frequency of C_l of cylinders in the both arrays are 2 because the vortices start to shed when $KC = 5$. The arrays of three and four cylinder have the same subharmonics. It is hard to compare the difference of C_l between arrays of three and four cylinders in the time domain. The spectrum analyses of C_l at $KC = 10$ in the different arrays are displayed in Fig. 19.



(a) The oblique oscillatory flow interacting with four cylinders.



(b) The horizontal oscillatory flow interacting with three cylinders in the symmetric configuration.

Fig. 15 Vorticity contours during a cycle, where $KC = 5$, $P/D = 2$, and $Re = 250$.

The ratios of fundamental frequency of C_i on the cylinder 1 in the both arrays are around 3. For cylinder 2, the ratios of fundamental frequency of C_i in the both arrays are close to 2.3. The amplitude of fundamental frequency of the same cylinder in the both arrays are equal. These results show that the frequency and am-

plitude of C_i are almost the same with that of the array of four cylinders.

CONCLUSIONS

The direct-forcing immersed boundary method was applied to the simulation of an oscillatory flow

past arrays of three cylinders in a regular triangle arrangement. In this study, there are a number of major results that are summarized in the followings.

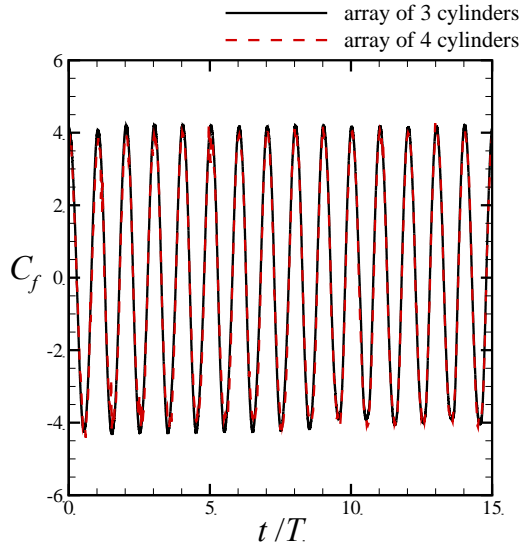


Fig. 16 Time histories of C_f in the different cylinder arrays in oscillatory flow for cylinder 2 at $P/D = 2$, $KC = 5$, and $Re = 250$.

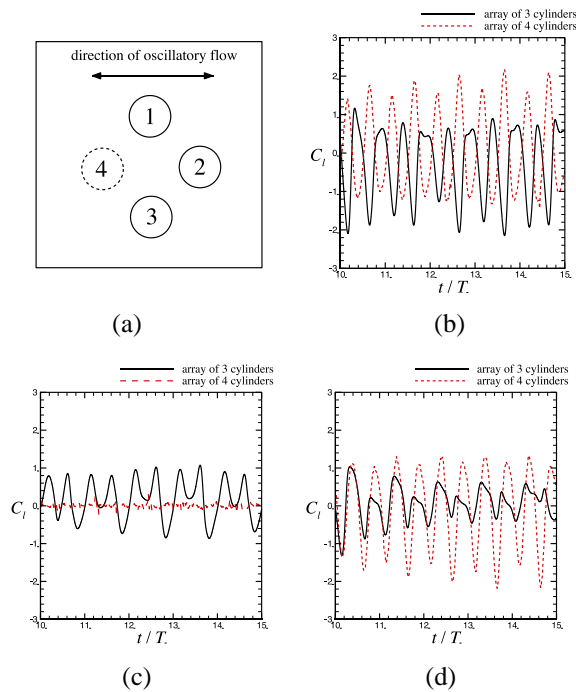
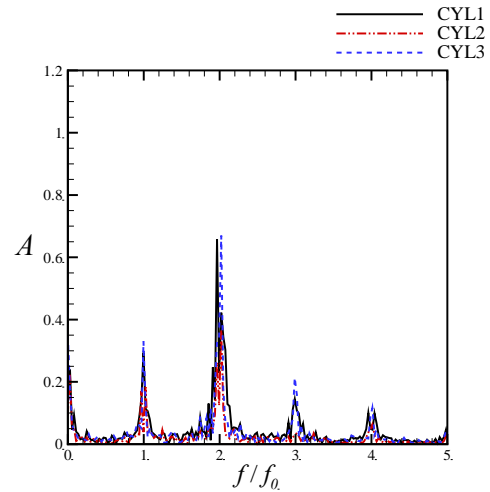
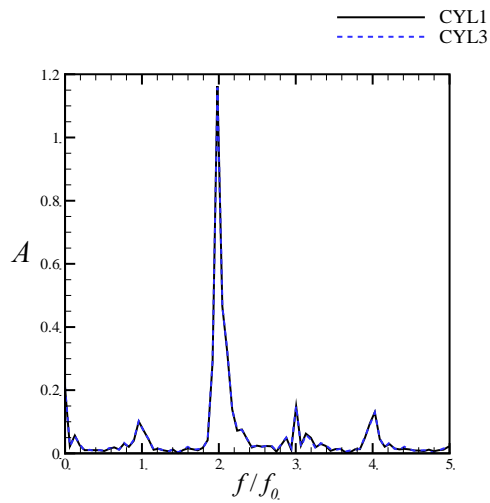


Fig. 17 Time histories of C_l in the different cylinder arrays in oscillatory flow at $P/D = 2$, $KC = 5$, and $Re = 250$: (a) schematics of cylinder arrays, (b) cylinder 1, (c) cylinder 2, and (d) cylinder 3.

The analysis for the KC number effect shows that more vortices occur and travel farther from the cylinders as the KC number increases. When the KC number exceeds a criterion, the symmetry of vortices around lateral cylinders is broken. Subsequently, the vortices of the central cylinder become asymmetric and shed from the cylinder. These asymmetric vortices cause an increase in the frequency of the transverse force coefficient C_l , leading to the appearance of more subharmonics in the C_l spectra. The difference between the amplitude of C_l for the lateral and central cylinders is more obvious as KC is low in the symmetric configuration. However, in-line force coefficients C_f of all cylinders are all inversely proportional to KC .



(a) Array of 3 cylinders.



(b) Array of 4 cylinders.

Fig. 18 Spectrum analyses of C_l at $P/D = 2$, $KC = 5$, and $Re = 250$.

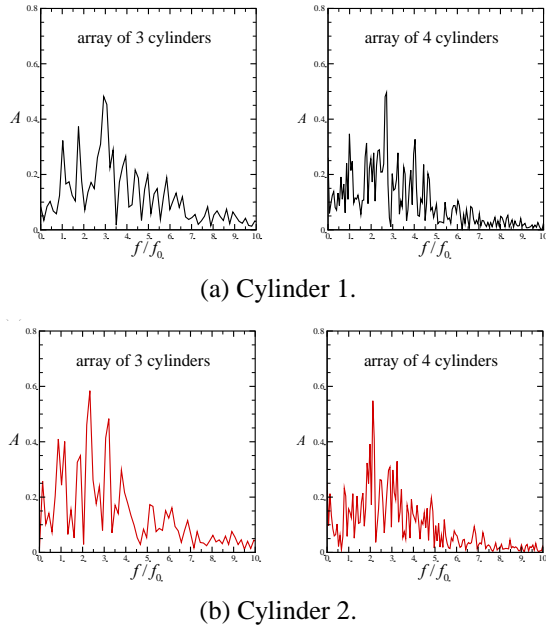


Fig. 19 Spectrum analyses of C_l on the cylinders in the different arrays at $P/D = 2$, $KC = 10$, and $Re = 500$.

The numerical results show that C_f of an array of three cylinders in the symmetric configuration is not affected by the pitch ratio P/D , but C_l and its fundamental frequency change with respect to P/D . As P/D decreases, the interaction among the three cylinders becomes strong. The root mean square value of C_l is similar to that of the single cylinder in the oscillatory flow as P/D increases.

At the same KC number, the interaction among three cylinders in the asymmetric configuration is stronger than that in the symmetric configuration. The asymmetric variation of vortices in asymmetric configuration is more obvious than the case of the symmetric configuration. C_f is not affected by the different configurations, but C_l of the three cylinders in the asymmetric configuration are higher than the case of the symmetric configuration.

In additions, the results of different arrays of three and four cylinders in the oscillatory flow are compared. The results show that C_f still remains the same in these different arrays. The amplitude and frequency of C_l in arrays of three and four cylinders are almost equal. Therefore, the results of C_f and C_l show that the array of three cylinders has the capability to replace the array of four cylinders in the tension-leg platform (TLP).

CONCLUSIONS

The three first-named authors would like to express gratitude for financial support from the Ministry of Science and Technology of Taiwan (Grant Nos: MOST 103-2221-E-011-110-MY3 and MOST 103-2115-M-035-001).

REFERENCES

1. Bao, Y., D. Zhou, and C. Huang, "Numerical simulation of flow over three circular cylinders in equilateral arrangements at low Reynolds number by a second-order characteristic-based split finite element method," *Comput. Fluids*, Vol. 39, pp. 882-899 (2010).
2. Sarpkaya, T., "Force on a circular cylinder in viscous oscillatory flow at low Keulegan-Carpenter numbers," *J. Fluid Mech.*, Vol. 165, pp. 61-71 (1986).
3. Obasaju, E.D., P.W. Bearman, and J.M.R. Graham, "A study of forces, circulation and vortex patterns around a circular cylinder in oscillation flow," *J. Fluid Mech.*, Vol. 196, pp. 467-494 (1988).
4. Sumer, B. and J. Fredsoe, *Hydrodynamics Around Cylindrical Structures*, Chapter 3, World Scientific Publishing, Singapore (1997).
5. Iliadis, I., and P. Anagnostopoulos, "Viscous oscillatory flow around a circular cylinder at low Keulegan-Carpenter numbers and frequency parameters," *Int. J. Numer. Methods Fluids*, Vol. 26, pp. 403-442 (1998).
6. An, H., L. Cheng, M. Zhao, and G. Dong, "Numerical simulation of the oscillatory flow around two cylinders in tandem," *J. Hydrodyn.*, Vol. 1, pp. 191-197 (2006).
7. Chern, M.J., P.R. Kanna, Y.J. Lu, and I.C. Cheng, "A CFD study of the interaction of oscillatory flows with a pair of side-by-side cylinders," *J. Fluids Struct.*, Vol. 26, pp. 626-643 (2010).
8. Anagnostopoulos, P. and Ch. Dikarou, "Numerical simulation of viscous oscillatory flow past four cylinders in square arrangement," *J. Fluids Struct.*, Vol. 27, pp. 212-232 (2011).
9. Chern, M.J., W.C. Hsu, and T.L. Horng, "Numerical prediction of hydrodynamic loading on circular cylinder array in oscillatory flow using direct-forcing immersed boundary method," *J. Appl. Math.*, Article ID 505916, 16 pages (2012).
10. Zhong, Z. and K.H. Wang, "Modeling fully nonlinear shallow-water waves and their interactions with cylin-

- dricial structures,” *Comput. Fluids*, Vol. 38, pp. 1018-1025 (2009).
11. Peskin, C.S., “Flow patterns around heart valves: A numerical method,” *J. Comput. Phys.*, Vol. 10, pp. 252-271 (1972).
 12. Mohd. Yusof, J., “Interaction of massive particles with turbulence,” Ph.D. thesis, Cornell University, Ithaca, NY, USA (1996).
 13. Noor, D.Z., M.J. Chern, and T.L. Horng, “An immersed boundary method to solve fluid-solid interaction problems,” *Comput. Mech.*, Vol. 44, pp. 447-453 (2009).
 14. Chern, M.J., W.C. Hsu, and T.L. Horng, “Immersed boundary modeling for interaction of oscillatory flow with cylinder array under effects of flow direction and cylinder arrangement,” *J. Fluids Struct.*, Vol. 43, pp. 325-346 (2013).
 15. Kempe, T. and J. Frohlich, “Improved immersed boundary method with direct forcing for the simulation of particle laden flows,” *J. Comput. Phys.*, Vol. 231, pp. 3663-3684 (2012).
 16. Chern, M.J., N.Z. Noor, C.B. Liao, and T.L. Horng, “Direct-forcing immersed boundary method for mixed heat transfer,” *Commun. Comput. Phys.*, Vol. 18, pp. 1072-1094 (2015).
 17. Dean, R.G. and R.A. Dalrymple, *Water Wave Mechanics for Engineers and Scientists*, Chapter 4, World Scientific Publishing, Singapore (1991).

振盪流場與正三角形圓柱列交互作用直接施力沈浸邊界法

陳明志* 陳宇樓* 廖清標** 洪子倫***

*國立台灣科技大學 機械工程研究所

**逢甲大學 水利工程與資源保育學系

***逢甲大學 應用數學系

關鍵詞：直接力量沈浸邊界法，圓柱列，振盪流，流固耦合

摘 要

近年來流固耦合的問題在離岸工業上受到高度重視，其中較為常見的應用為利用圓柱列在振盪流場中模擬離岸工作平台在週期性海流衝擊下的影響。大部分的海洋工作平台都是利用多於一根的圓柱做為受到海流衝擊的骨架，然而採用三根圓柱的設計卻是相當少見的，所以本研究主要利用直接施力沈浸邊界法模擬振盪流與正三角形配置圓柱列的流固耦合現象。直接施力沈浸邊界法主要是將一虛擬力加入動量方程式中，透過固體與流體的動量差可得到此虛擬力，最後藉此求解此固體對流體造成的作用力。本篇研究將探討 Keulegan-Carpenter number (KC)、圓柱間距和圓柱配置對稱性對於流場的影響，最後還會比較三根圓柱列和四根圓柱列在振盪流中的差異，其中四根圓柱列的配置是與三根圓柱列相似的。本研究藉由分析振盪流流經三根圓柱模擬海洋工作平台，瞭解真實結構物與周圍流場的受力情形，可提供設計海洋平台者做為參考。

(Manuscript received Jun. 01, 2017,
Accepted for publication Aug. 19, 2017)